Title
Nanodomain Engineering in Ferroelectric Capacitors with Graphene Electrodes.

Journal
Nano letters, 16(10)

ISSN
1530-6984

Authors
Lu, Haidong
Wang, Bo
Li, Tao
et al.

Publication Date
2016-10-01

DOI
10.1021/acs.nanolett.6b02963

Peer reviewed

NANO LETTERS

Letter

pubs.acs.org/NanoLett

Nanodomain Engineering in Ferroelectric Capacitors with Graphene Electrodes

Haidong Lu,[†] Bo Wang,[‡] Tao Li,[†] Alexey Lipatov,[§] Hyungwoo Lee,[∥] Anil Rajapitamahuni,[†] Ruijuan Xu,[#] Xia Hong,[†] Saeedeh Farokhipoor,[⊥] Lane W. Martin,[#,▽] Chang-Beom Eom,[∥] Long-Qing Chen,[‡] Alexander Sinitskii,[§,¶] and Alexei Gruverman*[,†,¶]

[†]Department of Physics and Astronomy, University of Nebraska, Lincoln, Nebraska 68588, United States

[‡]Department of Materials Science and Engineering, Pennsylvania State University, University Park, Pennsylvania 16802, United States

[§]Department of Chemistry, University of Nebraska, Lincoln, Nebraska 68588, United States

[∥]Department of Materials Science and Engineering, University of Wisconsin-Madison, Madison, Wisconsin 53706, United States

[⊥]Zernike Institute for Advanced Materials, University of Groningen, 9747 AG Groningen, The Netherlands

[#]Department of Materials Science and Engineering, University of California, Berkeley, California 94720, United States

[▽]Materials Science Division, Lawrence Berkeley National Laboratory, Berkeley, California 94720, United States

[¶]Nebraska Center for Materials and Nanoscience, University of Nebraska, Lincoln, Nebraska 68588, United States

Supporting Information

ABSTRACT: Polarization switching in ferroelectric capacitors is typically realized by application of an electrical bias to the capacitor electrodes and occurs via a complex process of domain structure reorganization. As the domain evolution in real devices is governed by the distribution of the nucleation centers, obtaining a domain structure of a desired configuration by electrical pulsing is challenging, if not impossible. Recent discovery of polarization reversal via the flexoelectric effect has opened a possibility for deterministic control of polarization in ferroelectric capacitors. In this paper, we demonstrate mechanical writing of arbitrary-shaped nanoscale domains in thin-film ferroelectric capacitors with graphene electrodes facilitated by a strain gradient induced by a tip of an atomic force microscope (AFM). A phase-field modeling prediction of a strong effect of graphene thickness on the threshold load required to initiate mechanical switching has been confirmed experimentally. Deliberate voltage-free domain writing represents a viable approach for development of functional devices based on domain topology and electronic properties of the domains and domain walls.

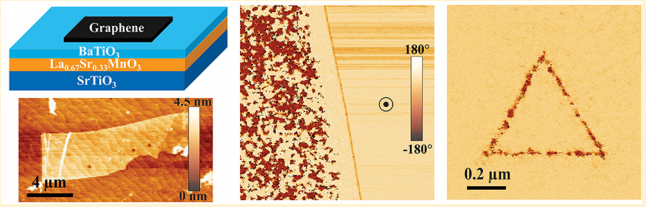

KEYWORDS: *Flexoelectric switching, graphene, domain engineering, ferroelectric films*

Polarization reversal in ferroelectrics under the action of an external electrical field is the most important aspect of their functional behavior. The mechanism of switching invariably involves a complex process of domain structure reorganization—domain nucleation, growth, and coalescence—which determines the performance of most of ferroelectric-based devices.[1] Application of ferroelectrics in memory devices is based on differentiation between two polarization states, which are used as logical bits. Functioning of recently proposed multilevel data storage devices, ferroelectric memristors,[2,3] depends on a ratio of oppositely oriented domains as a parameter controlling the device resistance. Also, recent research on domain walls as independent functional entities has shown that they possess physical properties distinct from those of the domains themselves.[4−8] These findings suggest that conceptually different ferroelectric devices with extended functionality can be explored by using domain topology, such as domain shape, domain size, domain walls density, and perimeter length, etc. Thus, accurate and arbitrary control of ferroelectric domains in ferroelectric capacitors is essential for exploring their emergent functionalities and realizing novel potential applications.

Polarization switching in ferroelectric capacitors is typically realized by application of an electric field that exceeds the coercive field of the material. Although in real devices domain evolution of 180° domains is not stochastic—it is typically governed by the defect structure of the ferroelectric medium[9]—local domain control in capacitors by electrical means cannot be realized, except for some special cases:[10] application of a voltage pulse to the electrodes results in multiple nucleation events leading to polarization reversal in the whole volume of the ferroelectric sandwiched between the electrodes. An electrically biased tip of an atomic force microscope (AFM) does allow

Received: July 16, 2016
Revised: September 16, 2016
Published: September 23, 2016

DOI: 10.1021/acs.nanolett.6b02963
Nano Lett. 2016, 16, 6460−6466

local electrical control of polarization, but only on a bare ferroelectric surface without the top electrode.[11,12] Hence, obtaining a domain structure of a specific configuration in a ferroelectric capacitor by electrical pulsing is challenging, if not impossible. On the other hand, recent discovery of a new polarization switching approach—via the flexoelectric effect—has enabled voltage-free control of polarization at the nanoscale.[13] Flexoelectric switching exploits a high strain gradient generated by the AFM tip pressed against the ferroelectric film surface,[14] which produces an electric field strong enough to overcome the coercivity of the film. Importantly, this mechanism provides a possibility for local polarization control in ferroelectric capacitors, since the strain gradient can be induced even in the presence of a top electrode. In this paper, we report the deterministic nanoscale control of polarization and domain engineering in $BaTiO_3$ thin-film capacitors with graphene electrodes by means of flexoelectric switching. Phase-field modeling predicts a strong effect of graphene thickness on the threshold mechanical load required for polarization reversal, which is consistent with the experimental data. The obtained results represent the first demonstration of deterministic domain control and domain-wall engineering in ferroelectric capacitors. This approach may further advance realization of a multilevel memory concept with mechanical writing and electrical reading of data.

To realize local control of polarization in ferroelectric capacitors, several issues have to be considered. First, the electric field strength due to a strain gradient generated by the AFM tip decreases with the distance from the surface; thus the top electrode should be thin enough (not more than a few nanometers according to our calculations below) to allow polarization switching in the ferroelectric film. Second, the same requirement holds for the ferroelectric film itself. Preliminary testing showed that the mechanical switching could be accomplished in the ferroelectric films as thick as 50 nm (see Figures S1 and S6 in the Supporting Information). Third, the electrode should be durable and complacent under a high mechanical load. From these considerations, epitaxial oxide electrodes, such as $SrRuO_3$, seem to be ideal for tip-induced flexoelectric switching. However, recent experimental studies showed that polarization screening by metal oxides is less effective than expected, which results in a progressive loss of the net polarization in ultrathin ferroelectric capacitors.[15,16] Typical metal electrodes used with ferroelectric capacitors, such as Pt, should be at least 10 nm thick to ensure good conductivity and mechanical durability, which might be too thick for mechanical switching. Here, we have chosen graphene as a top electrode material for the $BaTiO_3$ thin-film capacitors. This choice is based on the fact that graphene can be as thin as a single atomic carbon layer and that it is one of the strongest materials ever tested,[17] which would allow it to withstand a high tip-induced stress. Also, as a material with high carrier mobility and good electrical conductivity, graphene is an ideal material for electrodes. In our recent studies, we have demonstrated the use of graphene as an electrode in ferroelectric tunnel junctions, which allowed us to achieve reliable control of polarization and enhance the resistive switching behavior through interface engineering.[18]

For this study, the ferroelectric capacitors with graphene electrodes have been fabricated using $BaTiO_3$-based thin-film heterostructures ($BaTiO_3/La_{0.67}Sr_{0.33}MnO_3/SrTiO_3$) (Gr/BTO/LSMO). Epitaxial single-crystalline $BaTiO_3$ films with a thickness of 48 unit cells (u.c.) have been produced by pulsed-laser deposition on epitaxial $La_{0.67}Sr_{0.33}MnO_3$ layers grown on atomically smooth (001) $SrTiO_3$ substrates.[19] This type of substrate produces compressively strained $BaTiO_3$ films that possess only out-of-plane polarization.[20] Mechanically exfoliated graphene flakes were directly transferred onto the $BaTiO_3$ surface to form a Gr/BTO/LSMO capacitor (Figure 1a). Flakes

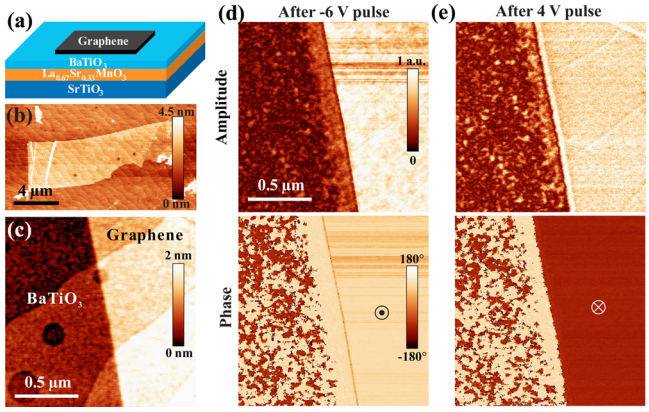

Figure 1. (a) A schematic view of the Gr/BTO/LSMO capacitor. (b) An AFM topographic image of a graphene flake on the $BaTiO_3$ surface. (c) AFM topographic image of the $BaTiO_3$ surface partially covered by graphene (on the right). (d–e) PFM amplitude (top) and phase (bottom) images after application of a −6 V voltage pulse (d) and a +4 V voltage pulse (e) to the graphene flake. Polarization underneath graphene has been fully switched upward or downward while polarization in the exposed $BaTiO_3$ remains intact.

composed of several graphene layers (from 1 to 5 layers) have been chosen for this study as they are sufficiently thin to allow stress extension into the underlying $BaTiO_3$ film (for details of graphene flakes characterization, see Figure S2 in the Supporting Information). Figure 1b shows an AFM image of the graphene flake on the $BaTiO_3$ surface. Detailed sample preparation information is given in the Materials and Methods Section.

Figure 1c–e demonstrates that conventional control of polarization in the Gr/BTO/LSMO capacitors by electrical means can be realized by applying a voltage pulse to graphene. Specifically, after voltage application, the resulting domain structures have been visualized by means of piezoresponse force microscopy (PFM).[21,22] PFM imaging around the graphene edge (Figure 1c) shows that the polarization state of $BaTiO_3$ underneath graphene can be completely switched up (Figure 1d) or down (Figure 1e), while the polarization state of the exposed $BaTiO_3$ film remains intact.

Results of the detailed study of domain structure evolution in the Gr/BTO/LSMO capacitors as a function of the applied bias are shown in Figure 2a. Voltage pulses of variable amplitude and fixed duration (1 s) were applied to induce polarization reversal. The onset of the switching process is characterized by homogeneous domain nucleation throughout the Gr/BTO/LSMO capacitor area followed by domain sidewise expansion. The maximum density of nucleation sites is estimated to be $\sim 400/\mu m^2$. The PFM phase images for different values of pulse amplitude have been converted to the switched capacitor areas allowing us to obtain a global PFM hysteresis loop (Figure 2b), which is analogous to the conventional polarization P–V hysteresis loops.[23] Significant asymmetry of the global PFM loop, which is also observed in the conventional (local) PFM loops (Figure S3 in the Supporting Information), is a

DOI: 10.1021/acs.nanolett.6b02963
Nano Lett. 2016, 16, 6460–6466

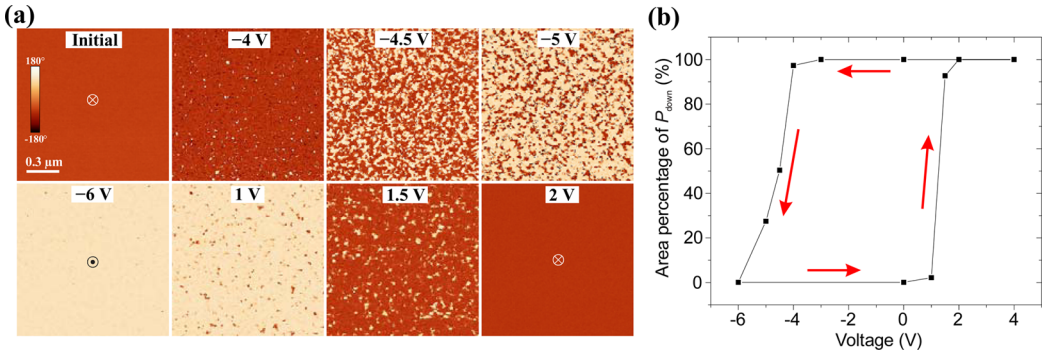

Figure 2. (a) PFM phase images of domain structures in the Gr/BTO/LSMO capacitor arising after application of voltage pulses of various amplitude and polarity to the graphene electrode. The images show a BTO film region completely covered by graphene. The pulse duration was set at 1 s. Homogeneous domain nucleation is observed in BTO underneath the graphene flake. (b) The switched downward domain area as a function of the pulse amplitude, showing typical ferroelectric hysteresis behavior.

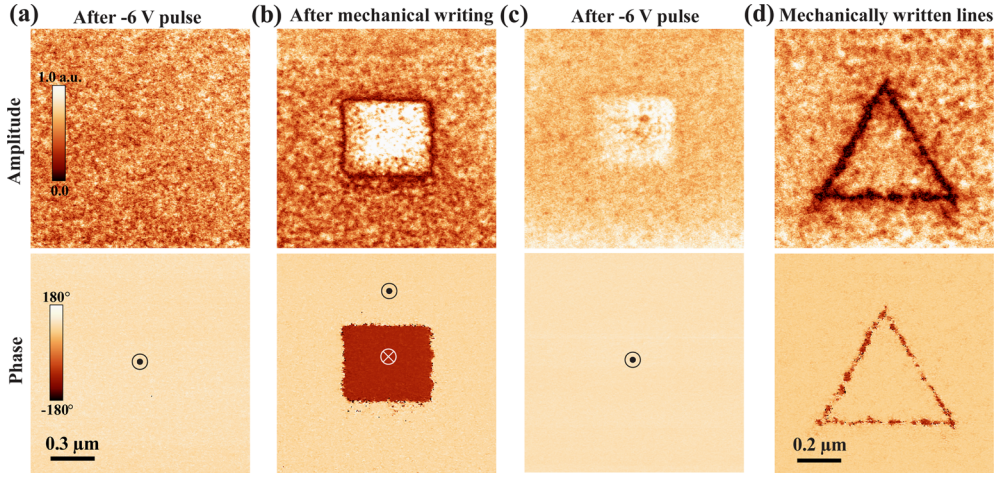

Figure 3. PFM images (top panel: amplitude; bottom panel: phase) of mechanical written domains in the Gr/BTO/LSMO capacitor. The images show BTO film regions completely covered by graphene. (a) An initial state with upward polarization. (b) The same area after scanning the central 500 × 500 nm^2 area with a grounded AFM tip held under 1.6 μN load. Polarization in the scanned area has been fully switched downward. (c) Electrical erasure of the mechanically written domain by a −6 V, 1 s electrical pulse. (d) Mechanically written nanodomain patterns.

manifestation of drastically different screening condition at the top (Gr/BTO) and bottom (BTO/LSMO) interfaces likely exacerbated by the presence of an adsorbate layer at the interface between graphene and BTO.[18]

Local control of polarization switching in the Gr/BTO/LSMO heterostructure is realized via the mechanical writing approach: the region underneath graphene surface that requires polarization switching is scanned by a grounded AFM tip held under a high mechanical load. A mechanical strain gradient generated by the AFM tip leads to polarization switching in the scanned region. Note that this approach can only switch polarization from the upward to the downward direction.[13] An initial upward polarization state in the Gr/BTO/LSMO heterostructure was generated by application of a −6 V pulse to the graphene flake (Figure 3a). Mechanical writing was performed by scanning a 500 × 500 nm^2 area with AFM tip under a 1.6 μN load, followed by conventional PFM imaging. Figure 3b shows the resulting domain pattern: the central 500 × 500 nm^2 area has been fully polarized downward while upward polarization outside this area remains intact. As mentioned above, in general, this type of location-specific polarization control cannot be realized via an electrical poling (Figure 2a). The mechanically poled area shows remarkable retention (at least several days without significant signs of relaxation) can be switched back simply by application of a negative voltage pulse to the graphene flake (Figure 3c). A "left-over" box with the higher amplitude at the location of the erased domain is likely due to removal of the interfacial adsorbate layer during mechanical poling (see discussion below and Figure 5), which ensures a better electrical contact between graphene and BTO. Mechanically induced transition from the upward to the downward polarization occurs via nucleation of a number of nanoscale domains with a domain nucleation density increasing upon the load increase until all domains coalesce. Figure S4 shows a series of transient domain structures, which develop in the Gr/BTO/LSMO heterostructure during scanning the graphene surface with the tip under various loads. This observation illustrates similarity between electrically and mechanically induced polarization reversal processes, although in the latter case the contribution of sidewise domain growth to switching seems to be less significant than in the former one.

Recently, it was shown that mechanically induced polarization reversal is more spatially localized than that due to the applied electrical field.[24] The localized nature of mechanical switching arises from a much smaller volume, over which mechanical stress is exerted by the AFM tip, in contrast to the volume affected by the electric field, which extends over

DOI: 10.1021/acs.nanolett.6b02963
Nano Lett. 2016, 16, 6460−6466

distances well beyond the tip−sample contact area. It can be assumed that the tip-generated stress should be also localized in the presence of a sufficiently thin top electrode, such as graphene, which would open a possibility of polarization control in the graphene-based ferroelectric capacitors with nanoscale precision. This feature is illustrated by Figure 3d, which shows PFM images of mechanically written triangular-shaped 20−40 nm wide domain lines in the Gr/BTO/LSMO heterostructure.

To get a better insight into mechanically induced polarization reversal in the Gr/BTO/LSMO heterostructures, we carried out phase-field modeling of the flexoelectric switching[25,26] using graphene thickness, t_{Gr}, as a variable with thickness values corresponding to 3, 6, 9, and 12 layers (assuming a commonly referred thickness of single-layer graphene of 3.4 Å). Other parameters used for modeling and a simulation setup illustrating a process of mechanically induced polarization reversal are shown in Figure 4a, and more details are provided

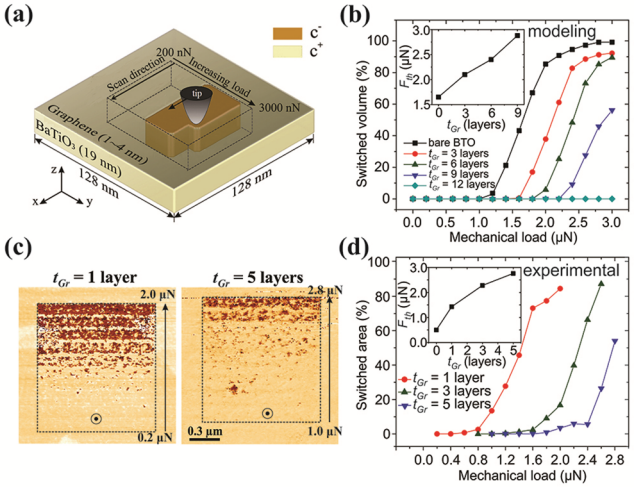

Figure 4. (a) A sketch diagram used for phase-field modeling of mechanical switching in Gr/BTO/LSMO capacitors by a scanning tip under pressure. The dashed area indicates an area subjected to mechanical load, which was increasing from 200 to 3000 nN. (b) Calculated volume of switched polarization as a function of mechanical load for different graphene thicknesses. Inset: graphene thickness dependence of the threshold load defined as the load required to switch 50% of polarization volume underneath the tip. Maximum graphene thickness that still allows mechanical switching by the load as high as 3 μN is equivalent to nine layers. (c) PFM images acquired in the Gr/BTO/LSMO heterostructure after mechanical domain writing by the AFM tip under an incrementally increasing load for two different graphene thicknesses. (d) Experimentally measured area of switched polarization as a function of mechanical load for different graphene thicknesses. Data are obtained from analysis of the PFM images in (c) (PFM image for t_{Gr} = 3 layers is not shown). The inset shows the graphene thickness dependence of the threshold load.

in Materials and Methods. The percentage of mechanically switched volume of $BaTiO_3$ underneath the tip calculated as a function of mechanical load is plotted in Figure 4b for different graphene thicknesses. It clearly predicts that, for t_{Gr} in the range from 0 to 9 layers, polarization reversal will occur as a result of an increasing mechanical load, while for t_{Gr} = 12 layers mechanical switching will not be possible. Also, it can be seen that the threshold load F_{th}, defined as the load required to switch 50% of polarization volume underneath the tip (similar to the definition of the local coercive field) becomes larger for thicker graphene. The calculated graphene thickness dependence of the threshold load is shown as inset in Figure 4b. The observed trend demonstrates that the existence of graphene electrode inhibits the mechanical switching in the $BaTiO_3$ film. Even a three-layer graphene flake (~1 nm thick) increases the threshold load by nearly 600 nN (Figure 4b) suggesting that the strain is concentrated in a small volume right underneath the tip.[14] The calculations predict that the maximum thickness of the graphene electrode allowing mechanical switching in the Gr/BTO/LSMO heterostructures is 9 layers (~3 nm) for the maximum load of 3 μN. Although mechanical switching may still be achievable with loads higher than 3 μN, such a high pressure typically leads to permanent damage (ripping) of graphene (Figure S5 in the Supporting Information).

The theoretical prediction of the threshold load increase with graphene thickness has been verified experimentally. Information on graphene flakes thickness has been obtained by AFM cross-section analysis and Raman spectroscopy (Figure S2 in the Supporting Information). Figure 4c shows the PFM phase images acquired after mechanical writing in the Gr/BTO/LSMO capacitors with graphene electrodes of different thickness, which illustrate the theoretically predicted trend: the onset of polarization reversal for monolayer graphene occurs at a much lower load than for 5 layers of graphene. More detailed studies shown in Figure 4d give clear evidence of a good agreement between experimental data and modeling results. Some minor qualitative discrepancy is observed for relatively small values of t_{Gr}, i.e., a threshold load predicted theoretically is higher than that measured experimentally (compare inset plots in Figure 4b and d). There are several factors that may contribute to this discrepancy. First, the exact flexoelectric coefficients for ultrathin $BaTiO_3$ films are still unknown. In the present study, we have used the ones from first-principle calculations (see Materials and Methods section for details). Second, the tip−sample contact area can only be estimated approximately.[27,28] Third, presence of an adsorbate layer at the graphene/$BaTiO_3$ interface, which was not taken into account during modeling, may affect the calculations. Indeed, Figure 5 shows a change in surface morphology of graphene as a result of applied mechanical load. Specifically, there is a depression with a depth of about 0.6 nm in the mechanically written square area, while the surrounding area has a height increase by up to about 0.4 nm. Remarkably, this topographic change gradually decreases with time, and eventually disappears, suggesting that there might be a fluidic

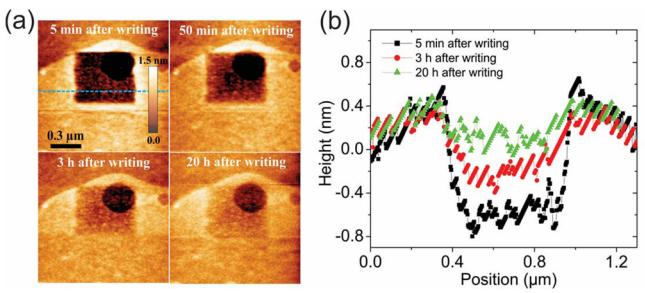

Figure 5. (a) AFM images of the Gr/BTO/LSMO capacitor showing topographic changes as a function of time after mechanical domain writing using a 1.6 μN load in the same square region as in Figure 3b. (b) The height profile along the blue line in (a) indicates a gradual decrease of the topographic depression with time. Note that the graphene flake is not damaged.

DOI: 10.1021/acs.nanolett.6b02963
Nano Lett. 2016, 16, 6460−6466

layer at the Gr/BTO interface, which can be squeezed out by mechanical load and can move back after the load is released.

Similar measurements on electrical and mechanical switching have been performed in $Pb(Zr,Ti)O_3$ films with graphene electrodes (Figures S7 and S8 in the Supporting Information) illustrating a general nature of the flexoelectric domain control, which therefore can be extended to other ferroelectric capacitors with ultrathin electrodes.

In conclusion, we have demonstrated controlled mechanical writing of arbitrary-shaped nanoscale domains in thin film ferroelectric capacitors with graphene electrodes facilitated by the flexoelectric effect due to a strain gradient induced by an AFM tip. Phase-field modeling of the flexoelectric switching is in good agreement with the experimental data. The obtained results demonstrate a feasibility of developing conceptually novel ferroelectric devices based on domain topology. Domains and domain walls of any configuration can be controllably created by means of mechanical switching, and electrically erased. Functionality of such devices will be determined not just by the polarization state (up or down) but also by domain size and domain walls configuration. For example, multilevel data storage devices based on electroresistance effect in the ferroelectric tunnel junctions[29] can be realized by gradual mechanically induced change in the volume faction of antiparallel domains allowing continuous tuning of device resistance from the OFF to the ON state. If instead domain wall conductivity is used as an active parameter,[8] the conductance of the device can be varied continuously by manipulating a density and perimeter length of the conducting domain walls connecting device electrodes making a tunable memristive device. Other functional properties of mechanically engineered domains and domain walls, such as superconductivity and magnetism, can be also employed to extend functionality of future devices.

Materials and Methods. *Sample Preparation.* Epitaxial single-crystalline $BaTiO_3$ films with thickness of 48 u.c. have been grown by pulsed laser deposition (PLD) on atomically smooth TiO_2-terminated (001)-$SrTiO_3$ substrates with a 30 nm thick $La_{0.67}Sr_{0.33}MnO_3$ layer as a bottom electrode. Before deposition, low angle miscut (<0.1°) $SrTiO_3$ substrates were etched using buffered HF acid for 60 s to maintain Ti-termination and then were annealed in oxygen at 1000 °C for 6 h to create atomically smooth surfaces with single-unit-cell-height steps. During deposition of all the layers, the substrate temperature was maintained at 680 °C with chamber oxygen pressure kept at 150 mTorr. The samples were cooled down to room temperature in oxygen atmosphere at 1 atm.

Graphene electrodes on $BaTiO_3$ surface were fabricated by means of mechanical exfoliation. To do so, flakes of highly oriented pyrolytic graphite (HOPG) were sandwiched between two pieces of Scotch tape so that their adhesive surfaces were facing each other. The two layers were then pressed firmly together and gently unfolded so that shiny graphite flakes remained on both pieces of tape. This process was repeated several times to obtain not shiny, but dark gray graphene flakes. Next, the $BaTiO_3$ film is pressed against the flake, and then the Scotch tape is gently peeled away leaving graphene flakes on the $BaTiO_3$ surface of film.

Characterization. Polarization imaging and local switching spectroscopy has been performed using a resonant-enhanced piezoresponse force microscopy (MFP-3D, Asylum Research). Conductive silicon cantilevers (PPP-EFM, Nanosensors) have been used in this study. PFM hysteresis loops were obtained at fixed locations on the heterostructure surface as a function of switching pulses (12 ms) superimposed on ac modulation bias with amplitude of 0.6 V_{p-p} at about 320 kHz. Tip contact forces have been calibrated by measuring force−distance curves and have been kept at a level of about 50−100 nN.

Phase-Field Modeling. As shown in Figure 4a, the Gr/BTO/LSMO heterostructure is modeled as a multilayer system sized by $128\Delta x \times 128\Delta x \times 40\Delta x$ grids where $\Delta x = 1$ nm. The thickness of BTO film (48 u.c.) and the substrate is set to be $19\Delta x$ and $13\Delta x$, respectively, while the thickness of graphene electrode ranges from 0 to $4\Delta x$. The temporal evolution of polarization in BTO ferroelectric film is described by time-dependent Ginzburg−Landau (TDGL) equation

$$\frac{\partial P_i(\mathbf{r}, t)}{\partial t} = -L\frac{\delta F}{\delta P_i(\mathbf{r}, t)} \quad (1)$$

where $P_i(\mathbf{r},t)$ is the polarization with respect to position $\mathbf{r}$ and time t, L is a kinetic coefficient, and F is the total free energy of the system. This equation is solved by semi-implicit Fourier method[30] with periodical boundary conditions in x and y directions, the details of which is elucidated in our previous works.[31] The Landau, elastic, electrostrictive and gradient coefficients used in the present phase-field modeling are identical with those in refs.[32,33] and the flexocoupling coefficients are adopted from the first-principles calculations.[34]

The biaxial compressive constraint exerted on BTO film by (001)-oriented STO substrate is 2.2%, calculated from the bulk lattice parameters at room temperature (a_{BTO} = 3.99 Å, a_{STO} = 3.905 Å). However, this homogeneous strain is partly relaxed by dislocations since the film thickness (~19 nm) is far larger than the critical thickness (~5 nm) of BTO/STO epitaxial films.[35] The effective homogeneous strain within 19 nm BTO film is computed to be 1.2% following the People−Bean model[36,37] and our earlier work.[38] The mechanical boundary condition at the bottom of substrate is displacement-free, while at the BTO surface is stress-free superposed by the distributions of applied stress σ_{33} and σ_{13} given by $\sigma_{13} = k\sigma_{33}$, where frictional coefficient k is assumed to be 0.25 for bare BTO case and 0 for graphene top electrode cases, and σ_{33} is consistent with our previous work.[26] For the tip movement, its position is set to move 5 nm along y axis every 2000 timesteps, accompanied by an increment of 200 nN loads starting from 200 to 3000 nN. After that, the applied stress is removed to have the simulated system relaxing for another 2000 timesteps.

An example of the calculated static domain structure under different load conditions applied to the BTO films through the top three-layer-thick graphene flake is shown in Figure S9 in the Supporting Information.

■ ASSOCIATED CONTENT

Supporting Information

The Supporting Information is available free of charge on the ACS Publications website at DOI: 10.1021/acs.nanolett.6b02963.

Supplementary Figures S1−S9. Figure S1: PFM images acquired after mechanical writing in the 48-u.c.-thick BTO film. Figure S2: AFM topographic and Raman spectroscopy data of the graphene flakes. Figure S3: PFM hysteresis loops. Figure S4: PFM images of BTO partially polarized by mechanical writing through graphene. Figure S5: AFM image of mechanically damaged graphene. Figure S6: Examples of mechanical switching

DOI: 10.1021/acs.nanolett.6b02963
Nano Lett. 2016, 16, 6460−6466

in other ferroelectric films. Figure S7: PFM images of the domain patterns in the Gr/PZT(50 nm)/LSMO. Figure S8: Illustration of both electrical and mechanical control of domain patterns in the Gr/PZT(50 nm)/LSMO. Figure S9: phase-field modeling of polarization reversal under tip-induced pressure (PDF)

AUTHOR INFORMATION

Notes

The authors declare no competing financial interest.

ACKNOWLEDGMENTS

The work at the University of Nebraska was supported by the U.S. National Science Foundation (NSF) through Materials Research Science and Engineering Center under Grant DMR-1420645 (thin film fabrication) and under Grant ECCS-1509874 (graphene fabrication and electrical characterization). A.G. and T.L. acknowledge the support by the Center for Nanoferroic Devices (CNFD), a Semiconductor Research Corporation Nanoelectronics Research Initiative (SRC-NRI) under Task ID 2398.002, sponsored by NIST and the Nanoelectronics Research Corporation (NERC). The work at University of Wisconsin-Madison was supported by the Army Research Office Grant W911NF-13-1-0486. The work at Pennsylvania State University (modeling) was supported by the NSF through Grants DMR-1210588. The computer simulations were carried out on the LION and cyberstar clusters at the Pennsylvania State University, in part supported by instrumentation (cyberstar Linux cluster) funded by the NSF through Grant OCI-0821527. X.H. and A.R. acknowledge the support by NSF CAREER Grant DMR-1148783. The work at the University of California, Berkeley, was supported by the National Science Foundation under Grants CMMI-1434147 (R.X.) and DMR-1451219 (L.W.M.).

REFERENCES

(1) Scott, J. F. Applications of Modern Ferroelectrics. *Science* **2007**, *315*, 954.
(2) Kim, D. J.; Lu, H.; Ryu, S.; Bark, C.-W.; Eom, C.-B.; Tsymbal, E. Y.; Gruverman, A. Ferroelectric Tunnel Memristor. *Nano Lett.* **2012**, *12*, 5697.
(3) Chanthbouala, A.; Garcia, V.; Cherifi, R. O.; Bouzehouane, K.; Fusil, S.; Moya, X.; Xavier, S.; Yamada, H.; Deranlot, C.; Mathur, N. D.; Bibes, M.; Barthélémy, A.; Grollier, J. A Ferroelectric Memristor. *Nat. Mater.* **2012**, *11*, 860.
(4) Seidel, J.; Martin, L. W.; He, Q.; Zhan, Q.; Chu, Y.-H.; Rother, A.; Hawkridge, M. E.; Maksymovych, P.; Yu, P.; Gajek, M.; Balke, N.; Kalinin, S. V.; Gemming, S.; Wang, F.; Catalan, G.; Scott, J. F.; Spaldin, N. A.; Orenstein, J.; Ramesh, R. Conduction at domain walls in oxide multiferroics. *Nat. Mater.* **2009**, *8*, 229.
(5) Guyonnet, J.; Gaponenko, I.; Gariglio, S.; Paruch, P. Conduction at Domain Walls in Insulating $Pb(Zr_{0.2}Ti_{0.8})O_3$ Thin Films. *Adv. Mater.* **2011**, *23*, 5377.
(6) Tybell, T.; Paruch, P.; Giamarchi, T.; Triscone, J.-M. Domain Wall Creep in Epitaxial Ferroelectric $Pb(Zr_{0.2}Ti_{0.8})O_3$ Thin Films. *Phys. Rev. Lett.* **2002**, *89*, 097601.
(7) Paruch, P.; Giamarchi, T.; Triscone, J.-M. Domain Wall Roughness in Epitaxial Ferroelectric $Pb(Zr_{0.2}Ti_{0.8})O_3$ Thin Films. *Phys. Rev. Lett.* **2005**, *94*, 197601.
(8) Catalan, G.; Seidel, J.; Ramesh, R.; Scott, J. F. Domain wall nanoelectronics. *Rev. Mod. Phys.* **2012**, *84*, 119.
(9) Gruverman, A.; Wu, D.; Scott, J. F. Piezoresponse Force Microscopy Studies of Switching Behavior of Ferroelectric Capacitors on a 100-ns Time Scale. *Phys. Rev. Lett.* **2008**, *100*, 097601.
(10) McGilly, L. J.; Yudin, P.; Feigl, L.; Tagantsev, A. K.; Setter, N. Controlling domain wall motion in ferroelectric thin films. *Nat. Nanotechnol.* **2015**, *10*, 145.
(11) Gruverman, A.; Kholkin, A. Nanoscale ferroelectrics: processing, characterization and future trends. *Rep. Prog. Phys.* **2006**, *69*, 2443.
(12) Kalinin, S. V.; Morozovska, A. N.; Chen, L. Q.; Rodriguez, B. J. Local polarization dynamics in ferroelectric materials. *Rep. Prog. Phys.* **2010**, *73*, 056502.
(13) Lu, H.; Bark, C.-W.; Esque de los Ojos, D.; Alcala, J.; Eom, C. B.; Catalan, G.; Gruverman, A. Mechanical Writing of Ferroelectric Polarization. *Science* **2012**, *336*, 59.
(14) Očenášek, J.; Lu, H.; Bark, C. W.; Eom, C. B.; Alcalá, J.; Catalan, G.; Gruverman, A. Nanomechanics of Flexoelectric Switching. *Phys. Rev. B: Condens. Matter Mater. Phys.* **2015**, *92*, 035417.
(15) Kim, D. J.; Jo, J. Y.; Kim, Y. S.; Chang, Y. J.; Lee, J. S.; Yoon, J.-G.; Song, T. K.; Noh, T. W. Polarization relaxation induced by a depolarization field in ultrathin ferroelectric $BaTiO_3$ capacitors. *Phys. Rev. Lett.* **2005**, *95*, 237602.
(16) Stamm, A.; Kim, D. J.; Lu, H.; Bark, C. W.; Eom, C. B.; Gruverman, A. Polarization relaxation kinetics in ultrathin ferroelectric capacitors. *Appl. Phys. Lett.* **2013**, *102*, 092901.
(17) Lee, C.; Wei, X.; Kysar, J. W.; Hone, J. Measurement of the Elastic Properties and Intrinsic Strength of Monolayer Graphene. *Science* **2008**, *321*, 385.
(18) Lu, H.; Lipatov, A.; Ryu, S.; Kim, D. J.; Zhuravlev, M. Y.; Eom, C. B.; Tsymbal, E. Y.; Sinitskii, A.; Gruverman, A. Ferroelectric Tunnel Junctions with Graphene Electrodes. *Nat. Commun.* **2014**, *5*, 5518.
(19) Eom, C. B.; Cava, R. J.; Fleming, R. M.; Phillips, J. M.; Van Dover, R. B.; Marshall, J. H.; Hsu, J. W. P.; Krajewski, J. J.; Peck, W. F. Single-Crystal Epitaxial Thin Films of the Isotropic Metallic Oxides $Sr_{1-x}Ca_xRuO_3$. *Science* **1992**, *258*, 1766.
(20) Choi, K. J.; Biegalski, M.; Li, Y. L.; Sharan, A.; Schubert, J.; Uecker, R.; Reiche, P.; Chen, Y. B.; Pan, X. Q.; Gopalan, V.; Chen, L.-Q.; Schlom, D. G.; Eom, C. B. Enhancement of ferroelectricity in strained $BaTiO_3$ thin films. *Science* **2004**, *306*, 1005.
(21) Gruverman, A.; Kalinin, S. V. Piezoresponse Force Microscopy and Recent Advances in Nanoscale Studies of Ferroelectrics. *J. Mater. Sci.* **2006**, *41*, 107.
(22) Bonnell, D. A.; Kalinin, S. V.; Kholkin, A. L.; Gruverman, A. Piezoresponse force microscopy: A window into electromechanical behavior at the nanoscale. *MRS Bull.* **2009**, *34*, 648.
(23) Wu, D.; Kunishima, I.; Roberts, S.; Gruverman, A. Spatial variations in local switching parameters of FeRAM capacitors. *Appl. Phys. Lett.* **2009**, *95*, 092901.
(24) Sharma, P.; Ryu, S.; Viskadourakis, Z.; Paudel, T. R.; Lee, H.; Panagopoulos, C.; Tsymbal, E. Y.; Eom, C. B.; Gruverman, A. Electro-Mechanics of Ferroelectric-like Behavior of $LaAlO_3$ Thin Films. *Adv. Funct. Mater.* **2015**, *25*, 6538.
(25) Gu, Y.; Li, M.; Morozovska, A. N.; Wang, Y.; Eliseev, E. A.; Gopalan, V.; Chen, L.-Q. Flexoelectricity and ferroelectric domain wall structures: Phase-field modeling and DFT calculations. *Phys. Rev. B: Condens. Matter Mater. Phys.* **2014**, *89*, 174111.
(26) Gu, Y.; Hong, Z.; Britson, J.; Chen, L.-Q. Nanoscale mechanical switching of ferroelectric polarization via flexoelectricity. *Appl. Phys. Lett.* **2015**, *106*, 022904.
(27) Fischer-Cripps, A. C. *Introduction to contact mechanics*, Mechanical Engineering Series, 2nd ed.; Springer: New York, 2007.
(28) Guo, E. J.; Roth, R.; Das, S.; Doerr, K. Strain induced low mechanical switching force in ultrathin $PbZr_{0.2}Ti_{0.8}O_3$ films. *Appl. Phys. Lett.* **2014**, *105*, 012903.
(29) Yamada, H.; Garcia, V.; Fusil, S.; Boyn, S.; Marinova, M.; Gloter, A.; Xavier, S.; Grollier, J.; Jacquet, E.; Carrétéro, C.; Deranlot, C.; Bibes, M.; Barthélémy, A. Giant electroresistance of super-tetragonal $BiFeO_3$-based ferroelectric tunnel junctions. *ACS Nano* **2013**, *7*, 5385.
(30) Chen, L. Q.; Shen, J. Applications of semi-implicit Fourier-spectral method to phase field equations. *Comput. Phys. Commun.* **1998**, *108*, 147.

DOI: 10.1021/acs.nanolett.6b02963
Nano Lett. 2016, 16, 6460−6466

(31) Li, Y. L.; Hu, S. Y.; Liu, Z. K.; Chen, L. Q. Effect of substrate constraint on the stability and evolution of ferroelectric domain structures in thin films. *Acta Mater.* **2002**, *50*, 395.
(32) Wang, J. J.; Wu, P. P.; Ma, X. Q.; Chen, L. Q. Temperature-pressure phase diagram and ferroelectric properties of $BaTiO_3$ single crystal based on a modified Landau potential. *J. Appl. Phys.* **2010**, *108*, 114105.
(33) Hlinka, J.; Márton, P. Phenomenological model of a 90° domain wall in $BaTiO_3$-type ferroelectrics. *Phys. Rev. B: Condens. Matter Mater. Phys.* **2006**, *74*, 104104.
(34) Ponomareva, I.; Tagantsev, A. K.; Bellaiche, L. Finite-temperature flexoelectricity in ferroelectric thin films from first principles. *Phys. Rev. B: Condens. Matter Mater. Phys.* **2012**, *85*, 104101.
(35) Sun, H. P.; Tian, W.; Pan, X. Q.; Haeni, J. H.; Schlom, D. G. Evolution of dislocation arrays in epitaxial $BaTiO_3$ thin films grown on (100) $SrTiO_3$. *Appl. Phys. Lett.* **2004**, *84*, 3298.
(36) People, R.; Bean, J. C. Calculation of critical layer thickness versus lattice mismatch for Ge_xSi_{1-x}/Si strained-layer heterostructures. *Appl. Phys. Lett.* **1985**, *47*, 322.
(37) People, R.; Bean, J. C. Erratum: Calculation of critical layer thickness versus lattice mismatch for Ge_xSi_{1-x}/Si strained-layer heterostructures. *Appl. Phys. Lett.* **1986**, *49*, 229.
(38) Sheng, G.; Hu, J.-M.; Zhang, J. X.; Li, Y. L.; Liu, Z. K.; Chen, L. Q. Phase-field simulations of thickness-dependent domain stability in $PbTiO_3$ thin films. *Acta Mater.* **2012**, *60*, 3296.

DOI: 10.1021/acs.nanolett.6b02963
Nano Lett. 2016, 16, 6460−6466